

Identified Particle Production from the BES at RHIC

Lokesh Kumar (for the STAR collaboration)
Physics Department, Kent State University, Kent, Ohio, USA

The RHIC Beam Energy Scan focuses on the study of the QCD phase diagram — temperature (T) vs. baryon chemical potential (μ_B). The aim is to verify some predictions from QCD: that a cross-over occurs at $\mu_B = 0$, that there exists a first-order phase transition at large μ_B and a critical point at an intermediate μ_B . The spectra and ratios of produced particles can be used to extract T and μ_B in different energies and system sizes. The STAR experiment has collected data for Au+Au collisions at $\sqrt{s_{NN}} = 7.7$ GeV, 11.5 GeV, and 39 GeV in the year 2010. We present midrapidity p_T spectra, rapidity density, average transverse mass, and particle ratios for identified hadrons from the STAR experiment. The centrality and transverse momentum dependence of the particle yields and ratios are compared to existing data at lower and higher beam energies. The chemical and kinetic freeze-out conditions are extracted from the ratios and particle spectra.

1. Introduction

The RHIC beam energy scan (BES) is devoted to exploring the QCD phase diagram [1–3]. The QCD phase diagram represents the variation of temperature T vs. baryon chemical potential μ_B . At low temperatures, the relevant degrees of freedom are expected to be hadronic but at high temperatures, the quarks and gluons are the relevant degrees of freedom of the system. In the QCD phase diagram, at $\mu_B \sim 0$, the transition from hadronic gas to quark gluon plasma (QGP) is expected to be a crossover [4]. At large μ_B , it is expected to be a first order phase transition [5]. The point where the first order phase transition line ends is called the QCD critical point which is of current interest for many heavy-ion experiments [1, 2, 6]. The main objectives of RHIC BES are to search for the possible QCD phase boundary and to search for the possible QCD critical point in the QCD phase diagram. In addition, it will be interesting to see how various observables, suggesting QGP formation at top RHIC energies, behave as the collision energy is decreased. This will help to locate the beam energy where there is no QGP formation or the energy representing “turn off” of the QGP signatures. A few potential observables for exploring the QCD phase diagram are: constituent-quark scaling of elliptic flow, parity-violation in strong interactions, wiggle shape of directed flow of protons, freeze-out eccentricity, K/π ratio fluctuations, and higher moments of net-protons [1].

The QCD phase diagram can be accessed by varying temperature T and baryonic chemical potential μ_B . Experimentally this can be achieved by varying the colliding beam energy. A T - μ_B space point in the QCD phase diagram can be obtained from the spectra and ratios of the produced hadrons. Once the T - μ_B space point is obtained, one can study various signatures, mentioned above, for evidence of the possible QCD phase boundary and QCD critical point. In the year 2010, the STAR experiment collected data for Au+Au collisions at energies $\sqrt{s_{NN}} = 7.7$, 11.5, and 39 GeV, as part of the proposed energies for the BES program, in addition to usual energies of 62.4 and 200 GeV.

2. Data Analysis

The data presented here are for Au+Au collisions at $\sqrt{s_{NN}} = 7.7$, 11.5, and 39 GeV taken in 2010 by the STAR experiment [7]. The total events analyzed for the results presented here are about 4 M, 8 M, and 10 M, respectively for $\sqrt{s_{NN}} = 7.7$, 11.5, and 39 GeV. The trigger selection is done by using the Beam Beam Counter (BBC) and the Vertex Position Detector (VPD) [8]. The main subsystem used for particle identification is the Time Projection Chamber (TPC) [9]. The particle identification is enhanced to higher p_T with the inclusion of the full barrel Time Of Flight (TOF) detector [10]. The centrality selection is done using the uncorrected charged track multiplicity measured event-wise in the TPC within $|\eta| < 0.5$. The centrality classes represent the fractions of this multiplicity distribution. The average number of participating nucleons ($\langle N_{part} \rangle$) and collisions ($\langle N_{coll} \rangle$) are obtained by comparing the multiplicity distribution with that from Glauber Monte Carlo simulation [2]. The raw yields are extracted at low p_T using ionization energy loss (dE/dx) from TPC, and using TOF information at higher p_T . The raw spectra are corrected for the detector acceptance and tracking efficiency. These correction factors are obtained together by embedding the tracks simulated using the GEANT model of the STAR detector into real events at the raw data level [11]. The results are presented for midrapidity $|y| < 0.1$ region.

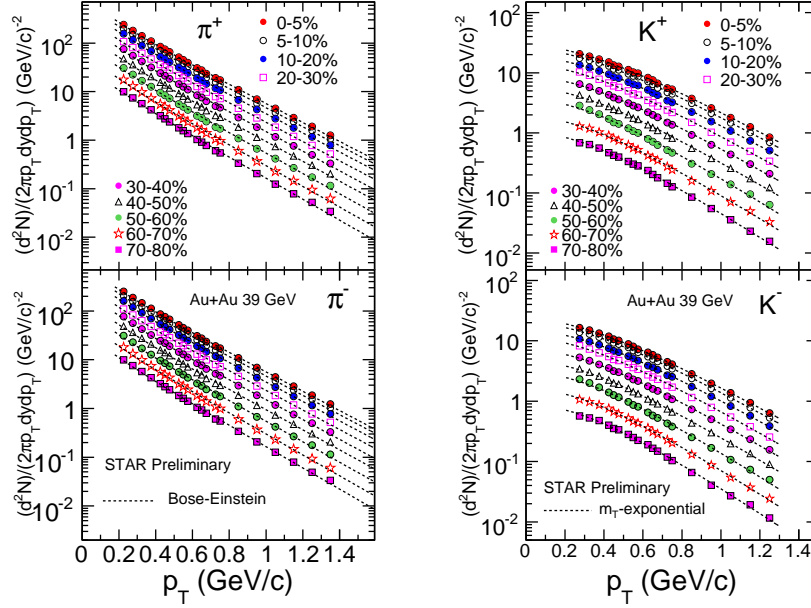


Figure 1: Transverse momentum spectra for charged pions π^\pm (left panel) and charged kaons K^\pm (right panel) for various collision centralities at midrapidity ($|y| < 0.1$) in Au+Au collisions at $\sqrt{s_{NN}} = 39$ GeV. Errors shown are statistical.

3. Results and Discussions

3.1. Transverse Momentum Spectra

Figure 1 shows invariant yields $d^2N/(2\pi p_T dy dp_T)$ vs. transverse momentum p_T for π^\pm (left panel) K^\pm (right panel) and for various collision centralities at midrapidity ($|y| < 0.1$) in Au+Au collisions at $\sqrt{s_{NN}} = 39$ GeV. The curves represent fits to the spectra: pion spectra are fitted with Bose-Einstein function and the kaon spectra with m_T -exponential. The dN/dy and $\langle p_T \rangle$ or $\langle m_T \rangle$ values are obtained using the data in the measured p_T ranges and extrapolating using a fit function (Bose-Einstein for π and m_T -exponential for K) for the unmeasured p_T ranges. The contribution to the yields from extrapolation to the total yield is about 20-30%. The pion spectra presented here are corrected for weak-decay feed-down and muon contamination using STAR HIJING+GEANT, as was done for previous STAR results [12]. The total contribution from weak-decay feed-down and muon contamination is about 17% at low p_T and becomes almost negligible ($\sim 1\%$) around $p_T = 1.4$ GeV/c.

3.2. Centrality Dependence of Yields and Average Transverse Momentum

Figure 2 shows the centrality dependence of dN/dy normalized by number of participating nucleon pairs $\langle N_{part} \rangle/2$ (top panels) and $\langle p_T \rangle$ (bottom panels) for π^\pm (left) and for K^\pm (right) in Au+Au collisions at $\sqrt{s_{NN}} = 7.7$ and 39 GeV. New measurements from BES data are compared to previously published results at top RHIC energies [12]. The dN/dy per participating nucleon pair for pions is almost constant as a function of collision centrality at $\sqrt{s_{NN}} = 7.7$ GeV, while it increases with N_{part} for higher energies and for kaons. The $\langle p_T \rangle$ increases with collision centrality for both pions and kaons at all energies, indicating that the average collective velocity in the radial direction increases with collision centrality.

3.3. Energy Dependence of Yields and Average Transverse Mass

Figure 3 shows the energy dependence of dN/dy normalized by $\langle N_{part} \rangle/2$ (top panels) and $\langle m_T \rangle - m$ (bottom panels) as a function of $\sqrt{s_{NN}}$ for π^\pm (left) and for K^\pm (right). The star symbols represent the data from BES energies and are compared with previous measurements [12–14]. The results are shown for the central collisions and for midrapidity regions. The STAR BES results are consistent with the published beam energy dependence

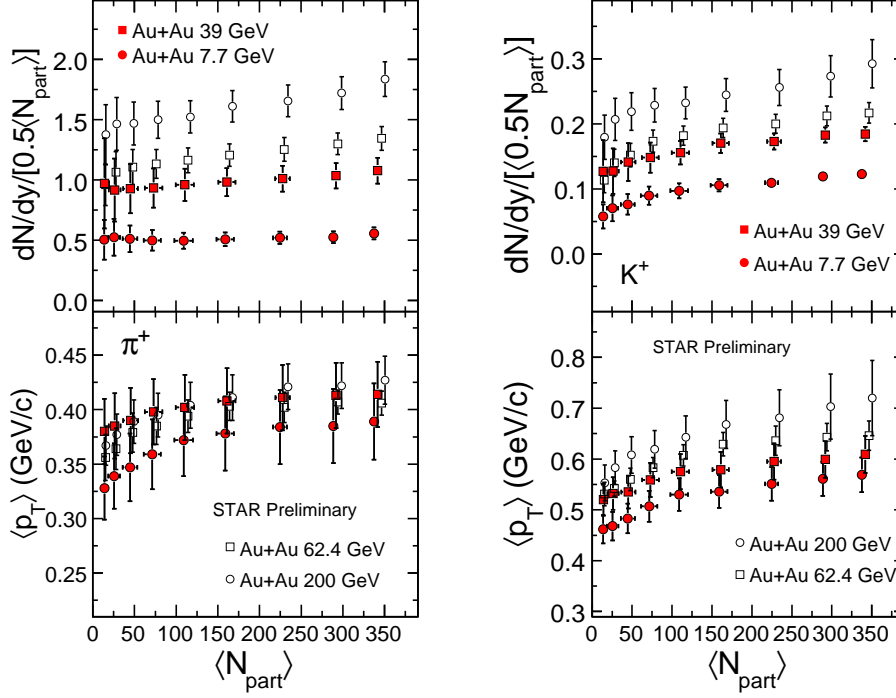


Figure 2: Left: Variation of dN/dy divided by participating nucleon pairs (top panel) and $\langle p_T \rangle$ (bottom panel) with collision centrality for π^\pm . Results from 7.7 and 39 GeV BES data are compared with those from previous STAR measurements [12]. Errors are statistical and systematic added in quadrature. Right: Similar measurements for K^\pm .

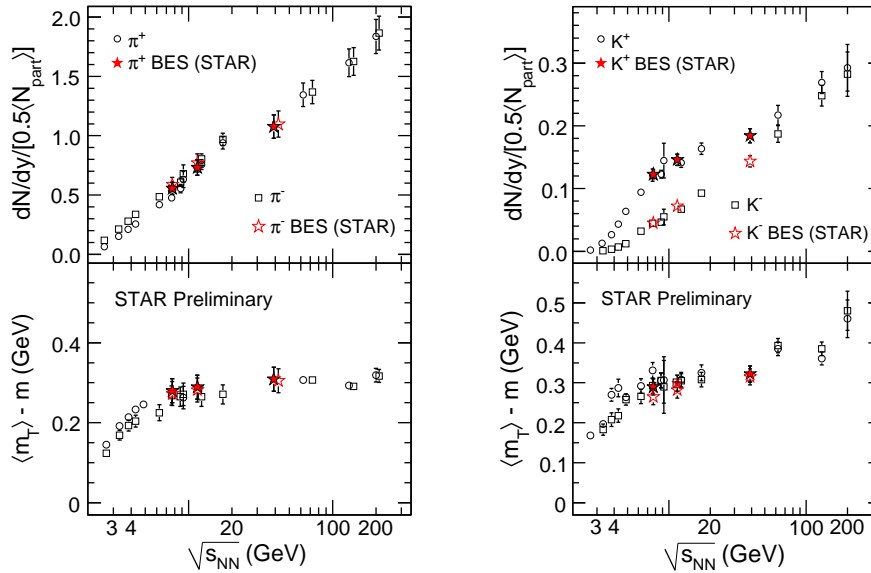


Figure 3: Left: dN/dy divided by participating nucleon pair (top panel) and $\langle m_T \rangle - m$ (bottom panel), plotted as a function of beam energy for π^\pm . Results from BES data are compared with those from previous measurements [12–14]. Errors are statistical and systematic added in quadrature. Right: Similar measurements for K^\pm .

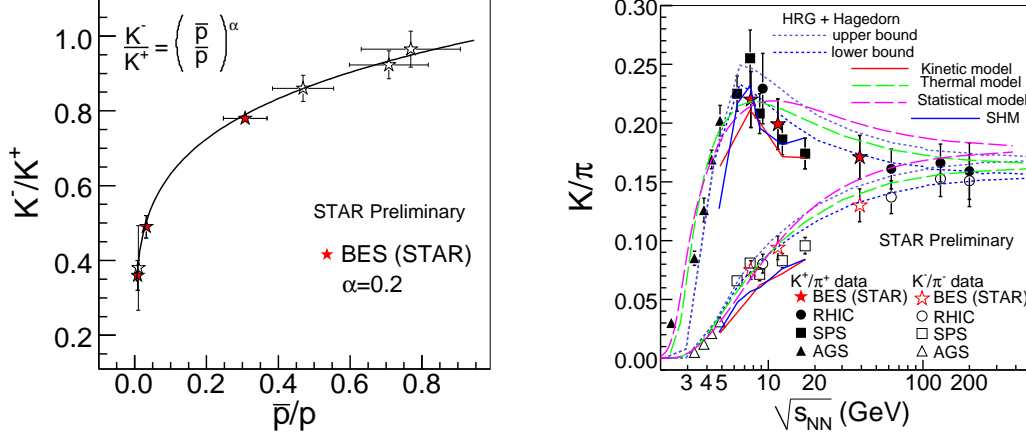


Figure 4: Left: Correlation of K^-/K^+ ratio with \bar{p}/p ratio for central collisions at midrapidity, shown for new measurements from BES data and for the published results from RHIC energies [12]. The curve represents a the power law fit to the data. Errors are statistical and systematic added in quadrature. Right: Energy dependence of K^\pm/π^\pm ratio for central collisions at midrapidity. New results from BES data are compared to previously published results at RHIC [12], SPS [13], and AGS [14]. Errors are statistical and systematic added in quadrature. Results are also compared with various theoretical model predictions [20–24].

trend. The yields per participating nucleon pair increase with beam energy. The quantity $\langle m_T \rangle - m$, where $m_T = \sqrt{p_T^2 + m^2}$ and m is the hadron mass, increases with beam energy for lower energies, becomes almost constant for the region covered by the BES data and then tends to increase towards the top RHIC energies. This is an interesting observation in a scenario where the system is in a thermodynamic state. In that case, $\langle m_T \rangle - m$ can be related to temperature of the system and dN/dy ($\propto \log(\sqrt{s_{NN}})$) may represent entropy. Then this observation could reflect the signature of a first order phase transition as proposed in the Ref. [15]. However, other interpretations of the observed $\langle m_T \rangle - m$ are possible [16].

3.4. Particle Ratios

The particle ratios provide useful information about the collision dynamics as these are fixed after the chemical freeze-out (see Sec. 3.5). Figure 4 (left panel) shows the correlation of K^-/K^+ ratio with \bar{p}/p ratio for new measurements from BES energies along with our previously published results [12]. This could give information on how the kaon production is related to the net-baryon density which is reflected by the \bar{p}/p ratio. The STAR p and \bar{p} yields are not feed-down corrected. At lower energies, the kaon production is dominated by the associated production which results in more K^+ production compared to K^- . Also the \bar{p}/p ratio is much less than unity at midrapidity, indicating that there is large baryon stopping at midrapidity at the lower energies. As we go towards higher energies, the pair production mechanism starts to dominate and the ratios tend to become closer to unity. The correlation between K^-/K^+ (representing net-strange chemical potential, μ_S) and \bar{p}/p (representing net-baryon chemical potential, μ_B) ratios seem to follow a power law behavior with $\alpha=0.2$ (represented by the curve). In a hadron gas, the relationship between μ_S and μ_B depends on the temperature. In a particular case of $T=190$ MeV and $\mu_B < 500$ MeV, these potentials follow the relation $\mu_S = (1/3)\mu_B$ [17].

Recent theoretical calculations [18] suggest that the maximum net-baryon density at freeze-out is attained at the lowest BES energy of $\sqrt{s_{NN}} \sim 7.7$ GeV. The maximum net-baryon density could also be related to the peak observed in the energy dependence of K^+/π^+ ratio at around $\sqrt{s_{NN}} \sim 7-8$ GeV, as was observed by the NA49 experiment [13]. This is sometimes referred to as the “horn”. The K/π ratio is also important as it could suggest the strangeness enhancement in heavy-ion collisions with respect to the elementary collisions. Figure 4 (right panel) shows the energy dependence of K^\pm/π^\pm ratio for central collisions at midrapidity. The BES results are shown with star symbols and are compared to results from previous measurements [12–14]. The BES results are in good agreement with the trend of energy dependence established by the published measurements.

Figure 4 (right panel) also shows the predictions of energy dependence of K/π ratio from various theoretical model calculations. The energy dependence of K^+/π^+ ratio has been interpreted using the Statistical Model of Early Stage (SMES) [19]. The model predicts first order phase transition and the existence of mixed phase

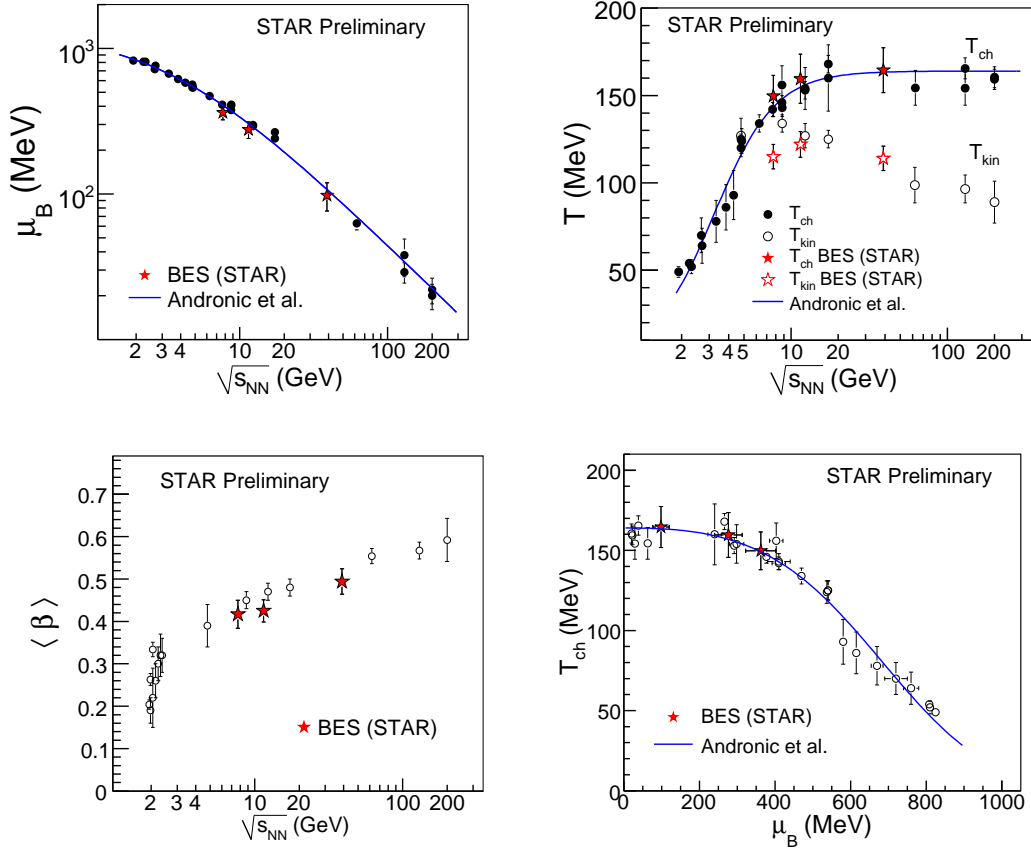


Figure 5: Energy dependence of baryonic chemical potential (top-left), temperature (T_{ch} , T_{kin}) (top-right), and average flow velocity (bottom-left). Bottom-right: Chemical freeze-out temperature plotted as a function of baryonic chemical potential. New results from BES data are shown with star symbols while other results are from the Ref. [12] and references therein. Curves represent the parametrization from Ref. [27].

around beam energy of 7-8 GeV. The SHM or Statistical Hadronization Model [20] assumes that the strong interactions saturate the particle production matrix elements. This means that the yield of particles is controlled predominantly by the magnitude of the accessible phase space. The system is in chemical non-equilibrium for $\sqrt{s_{NN}} < 7.6$ GeV, while for higher energies, the over-saturation of chemical occupancies is observed. The Statistical Model [21] assumes that the ratio of entropy to T^3 as a function of collision energy increases for mesons and decreases for baryons. Thus, a rapid change is expected at the crossing of the two curves, as the hadronic gas undergoes a transition from a baryon-dominated to a meson-dominated gas. The transition point is characterized by $T=140$ MeV, $\mu_B=410$ MeV, and $\sqrt{s_{NN}}=8.2$ GeV. In the Thermal Model [22], the energy dependence of K^\pm/π^\pm is studied by including σ -meson, which is neglected in most of the models, and many higher mass resonances ($m > 2$ GeV/ c^2) into the resonance spectrum employed in the statistical model calculations. The hadronic non-equilibrium Kinetic model [23] assumes that the surplus of strange particles is produced in secondary reactions of hadrons generated in nuclear collisions. Then the two important aspects are the available energy density and the lifetime of the fireball. It is suggested that these two aspects combine in such a way to show a sharp peak for the strangeness-to-entropy or K/π ratio as a function of beam energy. In the Hadron Resonance Gas and Hagedorn model (HRG+Hagedorn) [24], all hadrons as given in PDG with masses up to 2 GeV/ c^2 are included. The unknown hadron resonances in this model are included through Hagedorn's formula for the density of states. The model assumes that the strangeness in the baryon sector decays to strange baryons and does not contribute to the kaon production. The energy dependence of K^\pm/π^\pm ratio seems to be best explained using HRG+Hagedorn model.

3.5. Freeze-out Conditions

The integrated yields of hadrons change only through the inelastic collisions. The point in time when these inelastic collisions stop is called the chemical freeze-out. After this stage, the particle ratios are frozen and the system can be described by the thermal equilibrium model [12, 25] which involves two main parameters T_{ch} and μ_B . The T_{ch} and μ_B are obtained by fitting the particle ratios with the thermal model. The point in time when the elastic collisions among the particles cease is called the kinetic freeze-out. The system can be described by the blast-wave (BW) formulation involving two main parameters T_{kin} and average flow velocity $\langle\beta\rangle$ [12, 26]. The T_{kin} and $\langle\beta\rangle$ are obtained by simultaneously fitting the invariant yields for π , K , and p with the blast-wave model.

Figure 5 shows the variation of extracted freeze-out parameters for central collisions. Top-left plot shows the energy dependence of baryonic chemical potential. It shows that μ_B decreases as the beam energy increases. This is expected since there are fewer net-baryons at midrapidity at higher energies because of less stopping of baryons at midrapidity at higher energies. Top-right plot shows the kinetic freeze-out (open symbols) and chemical freeze-out (solid symbols) temperature plotted vs. $\sqrt{s_{NN}}$. The chemical freeze-out temperature increases with energy and saturates at the higher energies, and kinetic freeze-out temperature decreases with beam energy after $\sqrt{s_{NN}} \sim 7.7$ GeV. Bottom-left plot shows the average flow velocity plotted vs. $\sqrt{s_{NN}}$. The $\langle\beta\rangle$ increases with beam energy. Bottom-right plot shows the current picture of the phase diagram (T_{ch} vs. μ_B). The new measurements from BES program now extend the μ_B range covered by the RHIC from 20–400 MeV.

4. Summary

In summary, bulk properties from the RHIC BES program are presented in this paper. The BES data are nicely fitted in the beam energy dependence trend established previously. The yields of identified hadrons increase with beam energy. The $\langle m_T \rangle - m$ is almost constant for the BES energies. The $\langle p_T \rangle$ increases with centrality reflecting collectivity increases with centrality. The net-baryon density plays an important role at the lower energies as seen in the energy dependence of K/π ratio, and the correlation between K^-/K^+ and \bar{p}/p ratios. The new measurements from the BES program extend the μ_B range covered by the RHIC from 20–400 MeV.

Acknowledgments

We thank the RHIC Operations Group and RCF at BNL, the NERSC Center at LBNL and the Open Science Grid consortium for providing resources and support. This work was supported in part by the Offices of NP and HEP within the U.S. DOE Office of Science, the U.S. NSF, the Sloan Foundation, the DFG cluster of excellence ‘Origin and Structure of the Universe’ of Germany, CNRS/IN2P3, FAPESP CNPq of Brazil, Ministry of Ed. and Sci. of the Russian Federation, NNSFC, CAS, MoST, and MoE of China, GA and MSMT of the Czech Republic, FOM and NWO of the Netherlands, DAE, DST, and CSIR of India, Polish Ministry of Sci. and Higher Ed. Korea Research Foundation, Ministry of Sci. Ed. and Sports of the Rep. Of Croatia, and RosAtom of Russia.

References

- 1 STAR Internal Note-SN0493, 2009, arXiv:1007.2613 [nucl-ex].
- 2 B. I. Abelev *et al.* (STAR Collaboration), Phys. Rev. C **81**, 024911 (2010); L. Kumar (STAR Collaboration), Nucl. Phys. A **830**, 275C (2009); B. Mohanty, Nucl. Phys. A **830**, 899C (2009). L. Kumar (STAR Collaboration), Nucl. Phys. A **862**, 125 (2011).
- 3 S. Gupta, X. Luo, B. Mohanty, H. G. Ritter, and N. Xu, Science **332**, 1525 (2011).
- 4 Y. Aoki *et al.*, Nature **443**, 675 (2006).
- 5 S. Ejiri, Phys. Rev. D **78**, 074507 (2008); E.S. Bowman and J. I. Kapusta, Phys. Rev. C **79**, 015202 (2009).
- 6 A. Laszlo (NA61/SHINE Collaboration), Nucl. Phys. A **830**, 559C (2009); C. Hohné (CBM Collaboration), Int. J. Mod. Phys. E **16**, 2419 (2007); A. N. Sissakian *et al.* (NICA Collaboration), J. Phys. G **36**, 064069 (2009).
- 7 K. H. Ackermann *et al.*, Nucl. Instr. Methods A **499**, 624 (2003).

- 8 W. J. Llope *et al.*, Nucl. Instr. Methods A **522**, 252 (2004).
- 9 M. Anderson *et al.*, Nucl. Instr. Methods A **499**, 659 (2003).
- 10 W. J. Llope (STAR TOF Group), Nucl. Instr. and Meth. B **241**, 306 (2005).
- 11 V. Fine and P. Nevski, in Proceedings of CHEP-2000, Padova, Italy, p. 143.
- 12 B. I. Abelev *et al.* (STAR Collaboration), Phys. Rev. C **79**, 034909 (2009); *ibid.* Phys. Rev. C **81**, 024911 (2010).
- 13 S. V. Afanasiev *et al.* (NA49 Collaboration), Phys. Rev. C **66**, 054902 (2002); C. Alt *et al.* (NA49 Collaboration), Phys. Rev. C **77**, 024903 (2008); *ibid.* **73**, 044910 (2006); T. Anticic *et al.* (NA49 Collaboration), Phys. Rev. C **69**, 024902 (2004).
- 14 L. Ahle *et al.* (E866 Collaboration and E917 Collaboration), Phys. Lett. B **490**, 53 (2000); *ibid.* **476**, 1 (2000); J. L. Klay *et al.* (E895 Collaboration), Phys. Rev. Lett. **88**, 102301 (2002).
- 15 L. Van Hove, Phys. Lett. B **118**, 138 (1982).
- 16 B. Mohanty *et al.*, Phys. Rev. C **68**, 021901 (2008) and references therein.
- 17 I. G. Bearden *et al.* (BRAHMS Collaboration), Phys. Rev. Lett. **90**, 102301 (2003); J. Cleymans *et al.* Z. Phys. C **57**, 135 (1993).
- 18 J. Cleymans *et al.*, Phys. Rev. C **74**, 047901 (2006).
- 19 M. Gaździcki, M. I. Gorenstein, Acta Phys. Pol. B. **30**, 2705 (1999).
- 20 I. Kuznetsova *et al.* J. Phys. G **35**, 044011 (2008).
- 21 J. Cleymans *et al.* Eur. Phys. J. A **29**, 119 (2006).
- 22 A. Andronic *et al.* Phys. Lett. B **673**, 142 (2009).
- 23 B. Tomasik *et al.* Eur. Phys. J. C **49**, 115 (2007).
- 24 S. Chatterjee *et al.* Phys. Rev. C **81**, 044907 (2010).
- 25 J. Adams *et al.* (STAR Collaboration), Nucl. Phys. A **757**, 102 (2005); P. Braun-Munzinger *et al.*, Phys. Lett. B **344**, 43 (1995).
- 26 E. Schnedermann *et al.*, Phys. Rev. C **48**, 2462 (1993).
- 27 A. Andronic *et al.*, Nucl. Phys. A **834**, 237 (2010).